INTERNATIONAL JOURNAL FOR NUMERICAL METHODS IN FLUIDS, VOL. 12, 101–124 (1991)

ON THE ACCURACY OF FINITE DIFFERENCE AND MODAL METHODS FOR COMPUTING TIDAL AND WIND WAVE CURRENT PROFILES

A. M. DAVIES

Proudman Oceanographic Laboratory, Bidston Observatory, Birkenhead, Merseyside L43 7RA, U.K.

SUMMARY

This paper deals with the comparative accuracy of using finite difference grids or a modal representation through the vertical in modelling tidally or wind wave induced current profiles.

A point model is used in the vertical, with a no-slip condition at the sea bed. In the finite difference approach the high-shear bottom layer is resolved using either a regular grid on a logarithmic or log–linear transformed co-ordinate or an irregular grid, varying in such a manner as to retain second-order accuracy. The accuracy of these various grid schemes is considered in detail.

The relative merits of using either the Crank–Nicolson or Dufort–Frankel time integration methods are considered; in the case of a fine grid in a high-viscosity region, some numerical problems are found with the Dufort–Frankel method.

An alternative approach to using a finite difference grid in the vertical, namely a modal (spectral) method, is described. The form of the modes is such that they can accurately resolve the high-shear bottom boundary layer.

Calculations show that the thickness of the bottom boundary layer in relation to the total water depth is important in determining the choice of grid transform and rates of convergence of solutions using finite difference or modal methods. However, for the majority of problems the modal solution is numerically attractive owing to its computational efficiency and the ease with which solution algorithms based upon it can be coded in vectorizable form suitable for the new generation of vector computers.

The influence of viscosity profile, its time variation and water depth upon tidally induced or wave induced currents is considered. Calculations suggest that near-bed measurements of tidal flow in shallow water together with associated modelling would enable appropriate formulations of eddy viscosity to be determined. Similar measurements, though using a laboratory flume, would be appropriate for wind wave problems.

KEY WORDS Finite difference Spectral Tidal wave Wind wave Crank–Nicolson Logarithmic transform

1. INTRODUCTION

Although the number of applications[1–10] of three-dimensional hydrodynamic models has increased in recent years, the majority of these models do not include the very-near-bed layer, where high current shear occurs. In general these models apply a slip condition at the sea bed, with the bed stress related to the current 1 m above the bed. Consequently, such models cannot determine the near-bed current profile and shear stress distribution, which are important in a number of problems, e.g. sediment transport.

Future three-dimensional shelf sea models which can resolve the bottom boundary layer are now being developed. However, it is not clear at present just what is the most computationally

0271–2091/91/020101–24$12.00

Received March 1989
Revised January 1990

efficient means (e.g. finite difference or modal) of computing current profiles in such models when it is necessary to accurately resolve the high-shear bottom boundary layer. Also, the problem of wave–current interaction and its influence upon bed stress is particularly important in sediment movement problems, and any numerical technique used in the vertical should be able to include an accurate representation of the highly sheared near-bed wave boundary layer.

In this paper the accuracy and computational efficiency of solutions using various finite difference grids in the vertical are compared with a significantly different approach in which the Galerkin method with an expansion of functions is used through the vertical (a modal/spectral method).

In the finite difference solution, enhanced resolution in the near-bed region is obtained using either a logarithmic or log–linear transformation through the vertical and a uniform finite difference grid. An alternative approach in which the grid varies in such a manner as to give fine resolution in the near-bed layer but retains second-order accuracy (the kappa grid developed by Noye[11, 12]) is also considered.

In the functional (spectral) model a basis set of eigenfunctions (modes) of the eddy viscosity profile is used to compute the current profile. These modes satisfy a no-slip bottom boundary condition, and their vertical form is such that they are highly sheared in the near-bed region. By this means they can accurately resolve the bottom boundary layer.

The development of these various numerical methods for representing the current profile in the vertical is considered in the next section. In Sections 3 and 4 the accuracy and computational efficiency of the various approaches are considered for currents at both tidal and wind wave period in various depths of water. The sensitivity of computed current profiles to the vertical profile of eddy viscosity and its time variability is also considered.

2. HYDRODYNAMIC EQUATIONS AND THEIR NUMERICAL SOLUTION

2.1. Hydrodynamic equations

For a single-point model in the vertical the governing hydrodynamic equations are given by

$$\frac{\partial u}{\partial t} - \gamma v = \frac{\partial P}{\partial x} + \frac{\partial}{\partial z}\left(\mu \frac{\partial u}{\partial z}\right), \tag{1}$$

$$\frac{\partial v}{\partial t} + \gamma u = \frac{\partial P}{\partial y} + \frac{\partial}{\partial z}\left(\mu \frac{\partial v}{\partial z}\right). \tag{2}$$

In these equations the Coriolis parameter γ is constant, with μ denoting the coefficient of eddy viscosity and P the externally applied pressure forcing.

For sinusoidal forcing at a single frequency ω we express the pressure gradients as

$$\frac{\partial P}{\partial x} = \omega F_x \cos(\omega t), \tag{3}$$

$$\frac{\partial P}{\partial y} = \omega G_y \cos(\omega t), \tag{4}$$

with F_x, G_y the amplitude of the external forcing.

In equations (1)–(4), u and v are the x- and y-components of the current, with z the vertical co-ordinate.

For tidal or wind wave induced flows a zero-stress surface boundary condition is applied; thus

$$\mu\frac{\partial u}{\partial z}=\mu\frac{\partial v}{\partial z}=0. \tag{5}$$

In contrast to other calculations[3,4] which have employed a slip condition at the sea bed, the primary aim of the present series of calculations is to investigate accurate means of resolving the bottom boundary layer which arises when a no-slip condition, namely

$$u=v=0, \tag{6}$$

is applied at the sea bed.

2.2. Numerical solution using a finite difference grid in the vertical

Several algebraic transformations exists in the literature which can be used to transform equations (1) and (2) in such a manner that the discretized form of the transformed equations on regular grids is physically equivalent to using a grid with enhanced resolution in the near-bed region.

Appropriate transformations, onto a co-ordinate s, are either logarithmic of the form

$$s=\ln(z/S_0)/\beta, \quad \text{with } \beta=\ln(z/h), \tag{7}$$

or log–linear of the form

$$s=\left[\ln\left(\frac{z}{S_0}\right)+\left(\frac{z-S_0}{S_*}\right)\right]\Big/\beta, \quad \text{with } \beta=\ln\left(\frac{h}{S_0}\right)+\frac{h-S_0}{S_*}. \tag{8}$$

In these transformations, h is the water depth and S_0 is a small parameter which removes the logarithmic singularity at $z=0$ and determines the degree of grid resolution in the near-bed region. The parameter S_* in the log–linear transformation is an arbitrary height above the sea bed over which the grid is essentially logarithmic.

It can be readily shown from (7) that

$$\frac{\partial}{\partial z}=\frac{1}{\chi}\frac{\partial}{\partial s}, \quad \text{with } \chi=S_0\beta e^{\beta s}. \tag{9}$$

Using equation (1) for illustrative purposes, transforming gives

$$\frac{\partial u}{\partial t}-\gamma v=\frac{\partial P}{\partial x}+\frac{1}{\chi}\frac{\partial}{\partial s}\left(\frac{\mu}{\chi}\frac{\partial u}{\partial s}\right). \tag{10}$$

The numerical solution of equation (10) can be readily accomplished using the Crank–Nicolson method in the time domain, with a finite difference grid in the vertical.

Thus at the kth grid point we have

$$\frac{U_k^{t+\tau}-U_k^t}{\tau}-\gamma V_k^{t+0\cdot5\tau}=\frac{\partial P^{t+\theta_1\tau}}{\partial x}+\frac{\theta_1 W_k}{\Delta^2}(\mu_k^t\bar{W}_k\delta U_k^{t+\tau}-\mu_{k-1}^t\bar{W}_{k-1}\delta U_{k-1}^{t+\tau})$$
$$+\frac{\theta_2 W_k}{\Delta^2}(\mu_k^t\bar{W}_k\delta U_k^t-\mu_{k-1}^t\bar{W}_{k-1}\delta U_{k-1}^t), \tag{11}$$

with $\delta U_k=U_{k+1}-U_k$ and Δ the vertical grid spacing. A staggered finite difference grid with respect to viscosity and flow has been used in the vertical (see Figure 1). Also, $W_k=1/\chi$ evaluated at u grid point k and $\bar{W}_k=1/\chi$ evaluated at the midpoint between u grid points $k+1$ and k (see Figure 1).

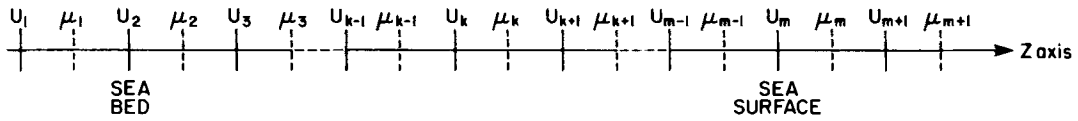

Figure 1. Finite difference grid in the vertical

In equation (11), θ_1 lies in the range $0 \leqslant \theta_1 \leqslant 1$, with $\theta_2 = 1{\cdot}0 - \theta_1$. In the Crank–Nicolson method the solution is time-centred with $\theta_1 = \theta_2 = 0{\cdot}5$.

An alternative to the Crank–Nicolson time integration method is to apply the Dufort–Frankel approach, which utilizes three time levels in the vertical (see Reference 13 for details). By this means an unconditionally stable method can be obtained by centring the diffusion term in time. Thus, considering a simple diffusion problem

$$\frac{\partial u}{\partial t} = \mu \frac{\partial^2 u}{\partial s^2},$$

the Dufort–Frankel method gives

$$\frac{u_k^{t+\tau} - u_k^{t-\tau}}{2\tau} = \frac{\mu}{\Delta^2}(u_{k+1}^t - u_k^{t+\tau} - u_k^{t-\tau} + u_{k-1}^t). \tag{12}$$

Obviously, this method can be readily applied to the discretization of equation (10) to yield a similar finite difference equation (see Reference 13 for details).

One problem with the Dufort–Frankel method is that odd and even time steps can become decoupled. This can, however, be avoided by applying some time filtering every n time steps, which serves to combine the solutions.

A simple but effective time filter[14] is of the form

$$\bar{F}(t) = F(t) + 0{\cdot}5\nu[F(t+\tau) - 2F(t) + F(t-\tau)], \tag{13}$$

where $\bar{F}(t)$ is the new time-filtered value of the current at time step t and ν is a weighting in the range $0 \leqslant \nu \leqslant 1$ which determines the extent of filtering. In the calculations presented later, $\nu = 0{\cdot}5$.

2.3. Numerical solution using a kappa grid in the vertical

Instead of using a transformation method with a regular finite difference grid to enhance grid resolution in the near-bed region, an irregularly spaced finite difference grid can be employed. In this case it can be shown[11, 12] that second-order accuracy can be retained in the vertical if the grid spacing changes such that

$$\Delta s_k = \Delta s_{k-1}(1 + \kappa \Delta s_{k-1}), \tag{14}$$

where Δs_k is the grid spacing between the $k+1$ and k points and κ is an arbitrary constant that determines how rapidly the grid changes. A high value of κ giving a coarse grid changing rapidly through the vertical to a fine one, whereas $\kappa = 0{\cdot}0$ represents a uniform grid.

A detailed discussion of finite difference methods based upon an irregular grid generated using recursion (12) (a kappa grid) can be found in the literature[11, 12] and will not be presented here. Also, the approach can be readily applied with the Crank–Nicolson method to discretize equation (10).

2.4. Numerical solution using the Galerkin method in the vertical

An alternative to using a finite difference grid in the vertical is to expand the two components of velocity, u and v, in terms of time-dependent coefficients $A_r(t)$, $B_r(t)$ and functions $f_r(s)$ in the vertical.

Thus

$$u=\sum_{r=1}^{m} A_r(t)f_r(s), \qquad v=\sum_{r=1}^{m} B_r(t)f_r(s), \tag{15}$$

where $s=z/h$ is a normalized (with respect to depth) vertical co-ordinate.

In general, the choice of basis functions $f_r(s)$ is arbitrary. However, in order to satisfy the no-slip boundary condition (equation (6)), the basis functions must be such that

$$f_r(0)=0 \quad \text{for all } r. \tag{16}$$

Consider for illustrative purposes equation (1). Applying the Galerkin method to this equation (see References 3–5 and 15 for details), transforming from z to s and integrating the term involving eddy viscosity by parts gives

$$\int_1^0 \frac{\partial u}{\partial t} f_k \,\mathrm{d}s = \gamma \int_1^0 v f_k \,\mathrm{d}s + \frac{\partial P}{\partial x}\int_1^0 f_k \,\mathrm{d}s + \frac{\mu}{h^2}\frac{\partial u}{\partial s} f_k\Big|_0 - \frac{\mu}{h^2}\frac{\partial u}{\partial s} f_k\Big|_1 - \frac{1}{h^2}\int_1^0 \mu \frac{\partial u}{\partial s}\frac{\mathrm{d}f_k}{\mathrm{d}s}\,\mathrm{d}s,$$

$$k=1, 2, \ldots, m. \tag{17}$$

Taking into account conditions (16) and (5), equation (17) simplifies to

$$\int_1^0 \frac{\partial u}{\partial t} f_k \,\mathrm{d}s = \gamma \int_1^0 v f_k \,\mathrm{d}s + \frac{\partial P}{\partial x}\int_1^0 f_k \,\mathrm{d}s - \frac{1}{h^2}\int_1^0 \mu \frac{\partial u}{\partial s}\frac{\mathrm{d}f_k}{\mathrm{d}s}\,\mathrm{d}s. \tag{18}$$

For the general case in which the eddy viscosity evolves through time, there is a significant computational advantage[3-5,15] in expressing μ in the form

$$\mu(z, t)=\sum_{j=1}^{m} E_j(t)\Phi_j(s), \tag{19}$$

with $\Phi_j(s)$ an arbitrary set of functions in the vertical.

Here we consider the much simpler case in which the eddy viscosity varies with time, although retaining a single functional form $\Phi(s)$ in the vertical; thus

$$\mu=\alpha(t)\Phi(s), \tag{20}$$

with α an arbitrary coefficient which can vary with horizontal position and time and can depend upon the current.

Substituting (15) and (20) into (18) gives

$$\sum_{r=1}^{m} \frac{\mathrm{d}A_r}{\mathrm{d}t}\int_1^0 f_r f_k \,\mathrm{d}s = \gamma \sum_{r=1}^{m} B_r \int_1^0 f_r f_k \,\mathrm{d}s + \frac{\partial P}{\partial x}\int_1^0 f_k \,\mathrm{d}s - \frac{\alpha}{h^2}\sum_{r=1}^{m} A_r \int_1^0 \Phi \frac{\mathrm{d}f_r}{\mathrm{d}s}\frac{\mathrm{d}f_k}{\mathrm{d}s}\,\mathrm{d}s, \quad k=1, 2, \ldots, m. \tag{21}$$

For the case in which Φ is independent of x, y and t, the m equations in (21) can be uncoupled by choosing the f_r to be eigenfunctions of

$$\frac{\mathrm{d}}{\mathrm{d}s}\left(\Phi\frac{\mathrm{d}f}{\mathrm{d}s}\right) = -\varepsilon f, \tag{22}$$

with ε-eigenvalues solved subject to boundary conditions that

$$\left.\frac{\mathrm{d}f_r}{\mathrm{d}s}\right|_1 = 0 \quad \text{and} \quad f_r(0) = 0. \tag{23}$$

For the case in which the basis functions f_r are eigenfunctions of (22), subject to boundary condition (23), equation (21) can be further simplified by taking advantage of the orthogonality property of eigenfunctions, namely

$$\int_1^0 f_r f_k \,\mathrm{d}s = 0, \quad r \neq k. \tag{24}$$

The eigenfunctions are also normalized such that their surface value is unity; thus

$$f_r(1) = 1, \quad r = 1, 2, \ldots, m.$$

Writing for convenience expansions (15) in the form

$$u = \sum_{r=1}^{m} A_r f_r = \sum_{r=1}^{m} u_r \psi_r f_r, \tag{25}$$

$$v = \sum_{r=1}^{m} B_r f_r = \sum_{r=1}^{m} v_r \psi_r f_r, \tag{26}$$

with $\psi_r = 1/\int_1^0 f_r f_r \,\mathrm{d}s$, equation (21) simplifies to

$$\frac{\mathrm{d}u_k}{\mathrm{d}t} = \gamma v_k + \frac{\partial P}{\partial x} a_k - \frac{\alpha}{h^2} \varepsilon_k u_k, \quad k = 1, 2, \ldots, m, \tag{27}$$

where $a_k = \int_1^0 f_k \mathrm{d}s$, with a corresponding equation

$$\frac{\mathrm{d}v_k}{\mathrm{d}t} = -\gamma u_k + \frac{\partial P}{\partial y} a_k - \frac{\alpha}{h^2} \varepsilon_k v_k. \tag{28}$$

These equations can be readily integrated through time and are unconditionally stable[5] if the viscosity term is centred in time; thus

$$\frac{U_k^{t+\tau} - U_k^t}{\tau} = \gamma V_k^{t+0.5\tau} + \frac{\partial P^{t+0.5\tau}}{\partial x} a_k - \frac{\alpha}{2h^2} \varepsilon_k (U_k^{t+\tau} + U_k^t), \quad k = 1, 2, \ldots, m. \tag{29}$$

Rearranging equation (29) gives

$$U_k^{t+\tau}\left(1 + \frac{\alpha\tau}{2h^2}\varepsilon_k\right) = \tau\left(1 - \frac{\alpha\tau}{2h^2}\varepsilon_k\right) U_k^t + \tau\gamma V_k^{t+0.5\tau} + \tau\frac{\partial P^{t+0.5\tau}}{\partial x} a_k, \quad k = 1, 2, \ldots, m. \tag{30}$$

Since the k equations in (30) are uncoupled and $U_k^{t+\tau}$ appears only on the left-hand side, this equation can be readily integrated using a simple forward time-stepping algorithm. The computational effort in solving the full three-dimensional hydrodynamic equations using m functions in the vertical is significantly less[16] than that involved using a similar number of grid boxes. Also, it has recently been shown[17] that such a method can be readily vectorized on a parallel computer to yield a particularly fast and computationally economic algorithm.

The modal method also yields significant insight (see References 5 and 18 for details) into the processes determining the current structure and the time variability of current. For example, if the term involving rotation is neglected in equation (27), we have

$$\frac{\mathrm{d}u_k}{\mathrm{d}t} = \frac{\partial P}{\partial x} a_k - \frac{\alpha}{h^2} \varepsilon_k u_k. \tag{31}$$

If we consider the case of a suddenly applied forcing $\partial P/\partial x$ in equation (31), which starts motion from rest, then initially each mode k is excited, with a weighting A_k determined by the values of ψ_k and a_k. Once excited, the modes decay with a decay time scale T_D given by

$$T_D = h^2/\alpha\varepsilon_k. \tag{32}$$

Since the eigenvalue ε_k increases (see Tables I and II) with mode number, higher modes are damped more rapidly than lower ones. Also, as expected, all modes are damped more rapidly if the average eddy viscosity α is increased. It is also interesting to note that the decay time increases as the square of the water depth, and consequently the effects of transients persist longer in deeper than in shallow water. The importance of the decay time T_D in understanding the time scale required to reach a periodic solution, and the influence of modal structure on current profiles, will be discussed in more detail in subsequent sections.

Table I. Comparison of computed and exact values of eigenvalues and eigenfunction derivatives at the sea bed with knot spacing shown, for a constant eddy viscosity of 1 $m^2 s^{-1}$

Eigenfunction (mode) number	Eigenvalue		Eigenfunction derivative at the sea bed	
	Numerical	Exact	Numerical	Exact
1	2·4674	2·4674	−1·5708	−1·5708
2	22·2066	22·2066	4·7124	4·7123
3	61·6851	61·6850	−7·8539	−7·8539
4	120·903	120·903	10·9955	10·9954
5	199·860	199·860	−14·1371	−14·1370
10	891·335	890·732	29·8563	29·8451
15	2110·94	2075·08	−45·6764	−45·5531

Knot spacing*

0·0 (0·05) 0·8 0·84 (0·02) 0·96 (0·005) 0·99 (0·0025) 0·995 (0·0005) 0·999 (0·0002) 0·9994 (0·0001) 0·9996 (0·00005) 0·9999 (0·00002) 0·99996 (0·00001) 0·99998 (0·000005) 1·0

* The knot spacing shown here is such that the first knot λ_0 (see Figure 3) is placed at zero, with subsequent knot intervals given by the term in brackets up to the knot positioned at 0·8. Other knot spacings and intervals follow the same convention.

Table II. Eigenvalues, normalized by dividing by the mean eddy viscosity α, and integrals of the modes (eigenfunctions) computed with eddy viscosity profile B (see Figure 2), with $\mu_1 = 0{\cdot}1\ m^2 s^{-1}$, $\mu_0 = 0{\cdot}0001\ m^2 s^{-1}$ and $h_1 = 0{\cdot}2h$, for $h = 10$ m. With these parameters the mean eddy viscosity $\alpha \approx 0{\cdot}09\ m^2 s^{-1}$

Eigenfunction (mode) number	Eigenvalue ε_r	Integral ψ_r	Integral a_r	$\left.\frac{\partial f_r}{\partial \sigma}\right\|_0$
1	0·738	1·262	0·882	−585·8
2	13·182	1·874	−0·082	967·5
3	44·779	1·778	0·038	−1517·0
4	89·985	1·628	−0·028	2291·1
5	149·655	1·712	0·019	−2627·1

3. NUMERICAL CALCULATIONS

3.1. Form of eddy viscosity

Since the principle aim of the calculations presented here is to compare the numerical accuracy of the functional and grid box approaches, it is instructive to consider a range of eddy viscosity formulations. Idealized profiles and time variations of viscosity are considered in the calculations to enable a clear and comprehensive comparison of the various approaches to be made.

The simplest profile of viscosity is one which is constant through the vertical (Figure 2, profile A). However, such a profile does not reflect the linear reduction in eddy viscosity which is known to occur in the near-bed region (Figure 2, profile B). Just over what distance the eddy viscosity increases in the near-bed region is difficult to assess. Measurements of Bowden and co-workers[19, 20] suggest that h_1 is of order 0·1–0·2 of the water depth. In profile B we fix $h_1 = 0{\cdot}2h$.

At the sea bed μ_0 is given by

$$\mu_0 = K_0 U_* Z_0,$$

where $K_0 = 0{\cdot}4$ is Von Karman's constant, U_* is the frictional velocity of order 2–4 cm s^{-1} and Z_0 is the roughness length of order 0·01–0·001 m, giving μ_0 of order 0·0001 m^2 s^{-1}.

Above the bottom boundary layer the eddy viscosity μ_1 is given by

$$\mu_1 = 0{\cdot}0025\, h|u|. \tag{33}$$

For strong tidal currents u is of order 1 m s^{-1}, and in typical shallow water depths of order 20 m equation (33) gives $\mu_1 = 0{\cdot}05$ m^2 s^{-1}.

An alternative formulation[4] is given by

$$\mu_1 = Ku^2/\sigma, \tag{34}$$

which, with $K = 2{\cdot}0 \times 10^{-5}$ and $\sigma = 10^{-4}$ s^{-1}, for $u = 1$ m s^{-1}, gives $\mu_1 = 0{\cdot}2$ m^2 s^{-1}.

In an initial series of calculations we take $\mu_1 = 0{\cdot}1$ m^2 s^{-1} as typical of the eddy viscosity away from the bottom boundary layer in a tidal flow of 1 m s^{-1}.

3.2. Eigenfunction accuracy

For the case in which the eddy viscosity is constant in the vertical, with a value α, the solution of the eigenvalue problem is given by

$$f_r = \cos(\lambda_r \sigma), \qquad \varepsilon_r = \lambda_r^2 \alpha,$$

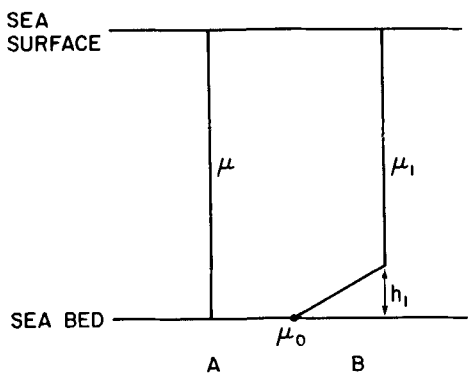

Figure 2. Profiles of eddy viscosity used in the calculations

with $\lambda_r = r\pi/2$, $r = 1, 3, 5, \ldots, \infty$. In this case the accuracy of the computed eigenfunctions can be readily checked by comparing them against the analytical solution.

Values of the eigenvalues and the vertical derivative of the eigenfunction at the sea bed (important in bed stress determination), computed using an expansion of fourth-order B-splines with the order of 60 knots in the vertical, are shown in Table I for $\alpha = 1\ m^2\ s^{-1}$. The fourth-order B-splines are piecewise polynomials which are non-zero only over a finite interval (Figure 3). Points along the z-axis at which the B-spline changes from zero to non-zero are termed knots, denoted by λ_i. Figure 3 shows the interval from sea surface to sea bed, divided into 10 interior knot segments. The number, position and separation of the knots are arbitrary and hence resolution can be increased in any region. The knot spacing was arranged such that it became very fine, of order 0·00005 of the water depth in the near-bed region (see Table I). It is evident that with this knot spacing, both the eigenvalues and the vertical derivative of the eigenfunction in the near-bed region could be accurately determined for the lower modes, with some slight error occurring in the higher ones. However, as we shall show later, it is the lower-order modes which contribute most to the solution.

It is interesting to note that when the eddy viscosity in the near-bed region is reduced, the vertical derivative increases (compare Tables I and II) and the modal structure is more highly sheared in the bed layer (Figure 4; compare profiles A and B). As we shall show later, this change in modal structure and bed shear is reflected in the computed current profiles.

3.3. Numerical calculations

Tidal wave of 12 h period, water depth $h = 10$ m. In an initial series of calculations the eddy viscosity did not vary with time and a specified profile A or B was used, with $\mu = 0{\cdot}1\ m^2\ s^{-1}$ for profile A and $\mu_1 = 0{\cdot}1\ m^2\ s^{-1}$, $\mu_0 = 0{\cdot}0001\ m^2\ s^{-1}$ for profile B.

Motion was driven by a unit pressure forcing of 12 h period (denoted by period D_2) in the x-direction, i.e. $F_x = 1{\cdot}0$, $G_y = 0{\cdot}0$, suddenly applied at time zero. Initially the effects of rotation were removed, i.e. $\gamma = 0{\cdot}0$ in equations (1) and (2). A time step of 3 min was used with the Crank–Nicolson method to integrate equation (1) forward in time; however, a stable solution for the current could be obtained with a time step of order 30 min, although the accuracy is reduced with such a large time step.[21]

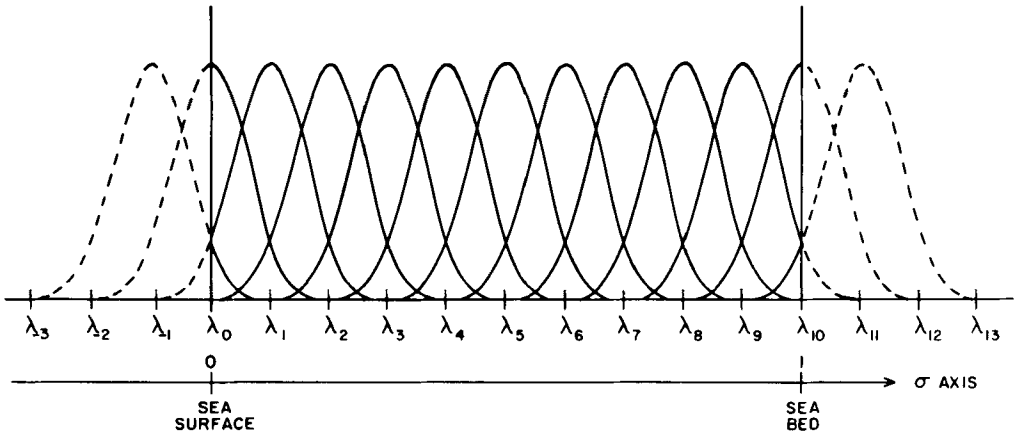

Figure 3. Distribution of B-splines and associated knots with depth

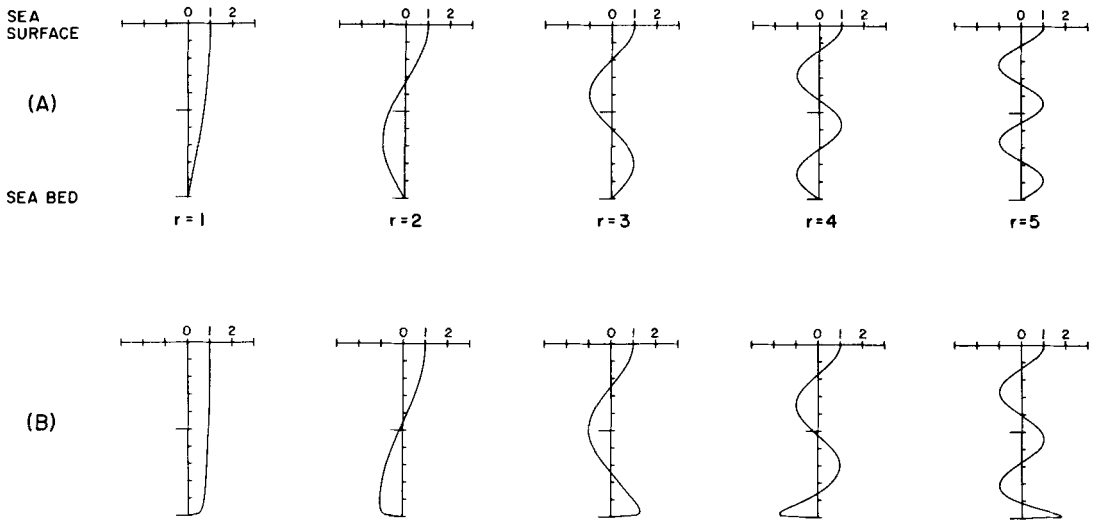

Figure 4. Vertical variation of the first five modes computed with viscosity profiles A and B

The Crank–Nicolson method was found to yield a stable and accurate solution with τ of order 12 min even when the eddy viscosity was high, $\mu = 0{\cdot}1\ \mathrm{m^2\,s^{-1}}$, at all depths (profile A, Figure 2), and a very fine grid (a logarithmic transform with $s_0 = 0{\cdot}0001$ m) was used close to the bed. Although a stable solution for the current profile could be obtained under these conditions, the near-bed currents showed some grid scale oscillations in the vertical and with time, giving time step oscillations in the bed stress. (A similar time step oscillation was found by Davies and Jones[21] in the bed stress computed with a turbulence energy model, but was cured with no loss of accuracy by arranging the turbulence production and dissipation terms in such a manner as to introduce some slight time smoothing.) By introducing some slight time filtering by applying the filter given in equation (13) at every 0·5 h in the tidal cycle, any oscillations in the bed stress were removed with no effect upon the current's accuracy.

The Dufort–Frankel method, although requiring some time filtering to couple together odd and even time steps, failed to produce a stable solution with $\mu = 0{\cdot}1\ \mathrm{m^2\,s^{-1}}$ and the fine logarithmic grid near the sea bed ($s_0 = 0{\cdot}0001$ m). In general the Dufort–Frankel method did exhibit instabilities (even with significant time smoothing, e.g. every three or four time steps) when the eddy viscosity was high in a fine-grid region (viscosity of order $0{\cdot}05\ \mathrm{m^2\,s^{-1}}$ with grid spacing Δs of order 0·001). The Crank–Nicolson method, however, proved very stable and was used in all grid calculations described in this paper. The excellent stability properties of the Crank–Nicolson method are supported by recent calculations of Lardner and Cekirge.[22]

Calculations using the modal model with the viscosity term centred in time (equation (30)) proved to be unconditionally stable for all viscosities, modal structures and time steps, and no time smoothing was required in any calculations using the modal approach.

Because motion was started from rest (zero initial current) by the sudden imposition of the forcing terms given in equation (3), it was necessary to integrate forward in time for the order of two tidal periods before the influence of these initial conditions was removed and the current became periodic. Once a periodic state was reached, a Fourier analysis was then performed using computed currents at each time step over a 12 h period in order to determine the amplitude and phase of the fundamental and, in the case of time-varying viscosity, the higher harmonics.

In the present case the eddy viscosity is time-invariant and consequently only the amplitude of the fundamental period (period D_2) was non-zero. However, in the case of a flow-dependent eddy viscosity (see later), other higher harmonics (denoted by D_4 having a period of 6 h and D_6 with a period of 3 h) could be generated.

Amplitudes and phases of the current at various heights z above the sea bed, computed using both the logarithmic and log–linear transforms with two different values of s_0 (the parameter determining the grid resolution in the near-bed layer), are shown in Table III. Also shown in this table are amplitudes and phases computed using the modal model.

It is evident from this table that when the eddy viscosity is constant in the vertical ($\mu = 0{\cdot}1\ m^2\,s^{-1}$), near-bed currents (i.e. within the bottom 1 m) are less than $1\ cm\,s^{-1}$. With $\mu = 0{\cdot}1\ m^2\,s^{-1}$ the flow is very viscous and the retarding influence of the bottom in a water depth of 10 m reaches the surface. The retarding influence of the bed was clearly evident in the surface current, the amplitude of which was only $5{\cdot}7\ cm\,s^{-1}$, which is significantly less than the

Table III. Amplitude h_0 ($cm\,s^{-1}$) and phase g_0 (deg) of near-bed tidal currents computed using a time-independent viscosity with profiles A and B in a water depth $h = 10$ m. Currents were computed using both grid boxes and modes through the vertical

	Log–linear ($s_0 = 0{\cdot}001$ m, $s_* = 5$ m) Number of grid boxes, N						Logarithmic ($s_0 = 0{\cdot}00001$ m) Number of grid boxes, N					
	10		20		60		10		20		60	
Height (m)	h_0	g_0	h_0	g_0	h_0	g_0	h_0	g_0	h_0	g_0	h_0	g_0
Viscosity profile A												
0·05	0·06	181	0·06	181	0·06	182	0·03	180	0·05	181	0·06	182
0·10	0·11	181	0·13	181	0·13	182	0·07	180	0·10	181	0·13	182
1·00	1·1	181	1·2	182	1·3	182	0·6	180	0·90	181	1·2	182
2·50	2·5	181	2·8	182	2·9	182	1·3	180	2·1	181	2·8	182
5·00	4·2	181	4·8	182	4·9	183	1·5	180	3·4	181	4·8	182
Viscosity profile B												
0·05	6·7	188	7·4	188	7·6	189	4·5	184	6·6	187	8·1	190
0·10	8·2	188	9·1	189	9·4	189	5·4	184	8·0	187	9·9	190
1·00	13·7	188	14·9	189	15·2	189	8·6	184	12·3	187	15·4	190
2·50	15·5	188	16·9	189	17·3	189	9·6	184	13·8	187	17·4	190
5·00	17·0	188	18·9	189	19·3	189	9·8	184	15·0	187	19·3	190

	Viscosity profile A Number of modes, M						Viscosity profile B Number of modes, M					
	5		10		15		5		10		15	
Height (m)	h_0	g_0	h_0	g_0	h_0	g_0	h_0	g_0	h_0	g_0	h_0	g_0
Eigenfunction solution												
0·05	0·07	182	0·07	182	0·07	182	9·2	191	9·2	191	9·3	191
0·10	0·14	182	0·14	182	0·14	182	11·1	191	11·2	191	11·1	191
1·00	1·4	182	1·4	182	1·4	182	17·4	191	17·4	191	17·4	191
2·50	3·2	182	3·2	182	3·2	182	19·6	192	19·6	192	19·6	191
5·00	5·4	182	5·4	183	5·4	182	21·9	192	21·9	192	21·8	191

100 cm s^{-1} which would occur if the flow was inviscid. In this calculation the thickness of the bottom boundary layer exceeded the water depth and the flow was sheared up to the surface. However, this shear was only gradual, namely 5·7 cm s^{-1} in 10 m.

It is evident from Table III that the solution computed using the log–linear transform converges very rapidly as the number of grid boxes, N, is increased in the vertical. The solution computed with $N=20$ was not significantly different from that computed with $N=60$. In the case of the logarithmic transformation a slower rate of convergence is evident (although that computed with $N=60$ is in good agreement with the log–linear transform). The logarithmic transformation used here gives a very fine grid spacing in the near-bed layer, with a significantly coarser spacing above. The effect of this is that when N is low (of order 10 or 20) there is insufficient resolution above the bed layer to adequately resolve the significant shear which still exists in the water column.

The modal solution was found to converge very rapidly, with currents computed with five modes identical to those computed with 15 modes (see Table III). In general, good agreement was obtained between the modal model and that computed using 60 grid boxes (see Table III) with either a logarithmic or log–linear transform, although currents computed with the modal model were slightly higher than those obtained with the grid box model.

As discussed earlier, solutions computed with a constant eddy viscosity, although an interesting test of the various methods, are not physically realistic. It is clear from Table III that when the eddy viscosity at the sea bed is reduced to 0·0001 $m^2 s^{-1}$, the near-bed current is enhanced. As in the previous example, solutions computed using the log–linear transform converge more rapidly than those based on a logarithmic transform, though solutions computed with 60 grid boxes in the vertical are not significantly different. Again the modal solution converges very rapidly; although the current magnitude is slightly higher than in the finite difference model, there is excellent agreement in the phase.

It is evident from these calculations that the log–linear grid for tidal problems appears to have some advantage over a logarithmic grid when the boundary layer occupies the total water column. However, the rate of convergence of the modal model is clearly much higher, and in problems where the shear layer extends though the water column it appears optimal.

Tidal wave of 12 h period, water depth $h=100$ m. In a physically realistic, three-dimensional simulation of tides on the continental shelf, a range of water depths from the order of 10–100 m will occur.

As shown in Section 2 and demonstrated in the previous calculation, modal convergence would be expected to be more rapid in a shallow than in a deep region. To check that an accurate solution can still be obtained using a modal expansion in deep water, the previous calculation was repeated in a water depth of 100 m. It is evident from Table IV that in such a water depth the sheared bottom boundary layer is only of the order of 25–50 m thick and hence, in contrast to the previous calculation, is only a fraction of the water column.

Again motion was started from rest; however, unlike in the previous case, four to five tidal cycles were required to obtain a steady state. The reason for this much slower decay of transients when $h=100$ m as opposed to $h=10$ m can be readily understood from equation (32). It is evident from this equation and Table II that the first mode has the slowest decay time scale, and also from Table II, a_r is largest for this mode and hence it is the dominant one.

From equation (32), taking $\alpha=0{\cdot}09$ $m^2 s^{-1}$, $\varepsilon_1=0{\cdot}738$ (Table II) and $h=100$ m gives a value of T_D of order 42 h, whereas with $h=10$ m, T_D is of order 0·42 h. This explains why approximately five tidal cycles (60 h) were required for transients to decay in a water depth of 100 m compared with a rapid adjustment in shallower water.

Table IV. Amplitude h_0 (cm s^{-1}) and phase g_0 (deg) of near-bed tidal currents with a time-independent viscosity in a water depth $h = 100$ m

	Log–linear ($s_0 = 0{\cdot}001$ m, $s_* = 50$ m) Number of grid boxes, N						Eigenfunctions Number of modes, M					
	10		20		60		5		10		15	
Height (m)	h_0	g_0	h_0	g_0	h_0	g_0	h_0	g_0	h_0	g_0	h_0	g_0
Viscosity profile A												
0·5	1·7	224	1·8	225	1·9	225	1·5	232	1·7	228	1·8	226
1·0	3·6	226	3·7	225	3·7	225	3·4	232	3·6	228	3·7	226
10·0	32·7	232	33·0	232	33·1	232	32·6	233	33·3	232	33·2	232
25·0	67·8	232	68·0	242	68·1	242	67·2	243	67·8	242	67·9	242
50·0	99·5	253	99·7	254	98·9	255	98·4	255	98·4	255	98·4	255
Viscosity profile B												
0·5	48·9	257	49·1	256	49·8	256	50·3	257	50·4	257	50·5	256
1·0	57·8	257	59·5	256	60·0	257	60·5	257	60·7	257	60·7	256
10·0	89·7	261	90·6	260	91·1	261	91·4	260	91·3	260	91·4	261
25·0	98·7	262	98·9	263	99·0	264	99·0	263	99·1	263	99·1	264
50·0	102·9	267	102·8	267	102·8	267	102·7	267	102·7	267	102·6	267

It is clear from Table IV that solutions (with profile A or B) computed using both the finite difference approach on a log–linear grid and the modal method converge very rapidly, with no significant difference in the solutions computed with the two methods. Again an accurate solution can be obtained using the order of five modes in the vertical, and the modal solution is probably optimal in this case in view of its low computational overhead and ability to code in a vectorizable form.[17]

Tidal flow with a time-dependent viscosity. In any physically realistic simulation, besides variations in water depth, the eddy viscosity would be expected to evolve with the flow field. In order to determine if using an eddy viscosity formulation given by equation (33) or (34) has a significant influence on the computed current, it is instructive to compute the tidal flow in both shallow ($h = 10$ m) and deep ($h = 100$ m) regions. Also as a check on the accuracy of the solution, and a comparison of the model with transformed grid and kappa grid in a physically realistic situation, these various methods were used in the calculation. Viscosity profile B was applied, with the viscosity given at any depth and time by

$$\mu(z, t) = \frac{f(\mu)}{\bar{\mu}}\mu(t)$$

with $f(\mu)$ the profile of viscosity (profile B, Figure 2, with $\mu_1 = 0{\cdot}1$, $\mu_0 = 0{\cdot}0001$) and $\bar{\mu}$ the vertically averaged value of μ, and $\mu(t)$ given by equation (33) or (34).

Such a separation into a time-independent function with a time-varying coefficient is of course an approximation. However, comparisons of computed and observed tidal profiles[3,4] using such a separation are in general in good agreement, thus justifying its use.

Since the eddy viscosity varies with time in these calculations, higher tidal harmonics and a mean flow can be generated. However, the time variation of the viscosity was such that only the second harmonic (D_6 having a period of 3 h) of the fundamental was produced.

Considering initially eddy viscosity related to the square of the flow, currents computed with five, 10 or 15 modes showed no significant differences. Computed profiles at 1 h intervals over a tidal cycle (see Figure 5) showed that using five modes it was possible to reproduce the high-shear bottom boundary layer and the near-linear variation of current with height above this layer. However, currents computed using 60 grid boxes in the vertical showed some slight differences depending upon whether a log–linear or logarithmic transform was used (see Table V). It is interesting to note that in many cases the modal solution lay between those computed with log–linear and logarithmic transforms, with five modes giving solutions of comparable accuracy to those computed using 60 grid boxes in the vertical.

Besides using a transformed grid in the vertical, it is instructive to examine the accuracy of the current profile determined using the kappa method. For small values of kappa ($\kappa < 5$), near-bed currents (the region below 1 m) were significantly lower (of order 3 cm s^{-1} for $h = 10$ m, 6 cm s^{-1} for $h = 100$ m) than those computed by the other methods, although at mid-depth (particularly when $h = 100$ m) they were not significantly different (see Table V). For higher values of kappa ($\kappa > 10$), near-bed currents were in better agreement with those computed using modes or transformed grids, although currents at mid-depth when $h = 10$ m were below those computed using the other methods.

The reason why near-bed currents are underestimated when $\kappa = 3{\cdot}5$ but are computed correctly when $\kappa = 14{\cdot}0$ is due to the fact that with a small value of κ the grid in the near-bed region is too coarse (see Table VI) and cannot accurately resolve the high shear which occurs in this area (see Table V). Increasing κ to 14·0 gives a fine grid close to the bed, enabling the shear layer to be accurately resolved, comparable with that obtained using a log–linear transformation with $s_0 = 0{\cdot}001$ (Tables V and VI). However, this value of κ does produce a very coarse grid higher in the water column (see Table VI) even when 100 grid boxes are used in the vertical. In the case of a water depth of 10 m, current shear occurs up to the water surface, and with this value of κ, currents at mid-depth cannot be accurately determined (Table V).

However, in the case of a water depth of 100 m, by mid-depth the flow is close to its free stream value of 100 cm s^{-1} and there is little shear in the water column (Table V); consequently a coarse

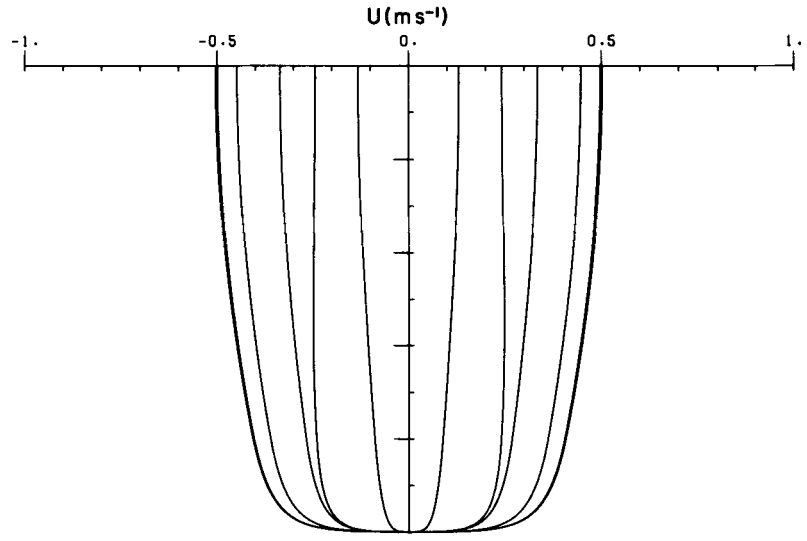

Figure 5. Current profiles at hourly intervals over a tidal period ($T = 12$ h), computed with five modes in the vertical

Table V. Amplitude h_0(cm s^{-1}) and phase g_0(deg) of near-bed tidal currents at the fundamental period (D_2) and the third harmonic (D_6) computed with a time-dependent eddy viscosity and viscosity profile B

Height (m)	$\mu \propto u^2$						Kappa				$\mu \propto hu$					
	Modes		Log–linear		Logarithmic		$\kappa = 3{\cdot}5$		$\kappa = 14{\cdot}0$		Modes		Log–linear		Logarithmic	
	h_0	g_0	h_0	g_0	h_0	g_0	h_0	g_0	h_0	g_0	h_0	g_0	h_0	g_0	h_0	g_0
Water depth $h = 10$ m																
D_2																
0·05	21·6	209	19·6	209	22·3	211	16·4	207	19·4	207	33·5	227	30·3	224	33·5	226
0·10	26·0	209	24·1	209	26·8	211	21·4	208	23·8	208	40·4	227	37·5	224	40·5	226
1·00	40·3	211	39·0	212	41·7	213	37·3	211	37·9	210	62·9	228	60·9	226	63·2	228
2·50	45·3	212	44·3	213	46·9	214	42·8	212	42·6	211	70·8	229	69·1	226	71·0	229
5·0	50·3	213	49·4	214	51·7	215	48·2	213	46·7	212	78·5	230	77·1	228	78·4	230
D_6																
0·05	2·6	118	2·4	113	2·6	121	2·1	106	2·5	109	1·3	179	1·3	176	1·3	181
0·10	3·2	120	3·0	116	3·2	124	2·7	110	3·1	112	1·6	181	1·6	178	1·6	184
1·00	4·9	133	5·0	129	5·1	136	4·9	125	5·1	124	2·7	200	2·9	196	2·8	202
2·50	5·6	140	5·8	136	5·9	142	5·7	132	5·9	130	3·2	210	3·5	206	3·4	211
5·0	6.3	147	6·6	142	6·7	148	6·5	140	6·6	135	3·9	222	4·3	217	4·2	221
			($s_0 = 0{\cdot}001$ m, $s_* = 5$ m)		($s_0 = 0{\cdot}0001$ m)								($s_0 = 0{\cdot}001$ m, $s_* = 5$ m)		($s_0 = 0{\cdot}00001$ m)	
Water depth $h = 100$ m																
D_2																
0·5	55·5	243	54·7	243	54·3	244	45·8	239	52·5	243	48·6	249	47·9	249	48·2	250
1·0	65·7	245	64·8	246	64·3	246	58·1	242	63·0	245	58·3	250	57·7	250	57·9	251
10·0	92·8	256	92·5	256	92·3	257	90·8	254	91·9	256	87·7	255	87·5	255	87·7	256
25·0	99·0	260	98·9	261	98·9	262	98·5	260	99·0	261	96·0	259	96·0	259	96·3	260
50·0	102·1	266	102·1	266	102·2	267	102·4	266	103·2	266	101·9	263	102·2	263	102·6	264
D_6																
0·5	7·0	218	7·1	218	7·0	209	7·4	213	7·4	215	3·1	210	3·0	209	3·0	199
1·0	7·2	223	7·0	225	6·8	218	7·8	221	7·4	224	3·4	214	3·3	214	3·2	205
10·0	3·5	277	3·6	277	3·3	272	4·3	273	3·8	273	2·5	251	2·4	249	2·3	246
25·0	2·3	319	2·2	319	2·0	319	2·6	315	2·1	320	1·6	285	1·6	285	1·5	285
50·0	1·4	16	1·4	18	1·3	45	1·6	17	1·7	29	1·1	228	1·1	227	1·2	357
			($s_0 = 0{\cdot}001$ m, $s_* = 50$ m)		($s_0 = 0{\cdot}0001$ m)								($s_0 = 0{\cdot}001$ m, $s_* = 50$ m)		($s_0 = 0{\cdot}0001$ m)	

Table VI. Height (m) above the bed of near-bed and near-surface grid points for a range of grid types computed with $N = 100$ grid boxes in the vertical in a water depth $h = 10$ m

	Height of near-bed point			Height of near-surface point		
Grid type	1	2	3	$N-3$	$N-2$	$N-1$
Kappa ($\kappa = 1{\cdot}0$)	0·063	0·126	0·190	9·505	9·667	9·832
Kappa ($\kappa = 14{\cdot}0$)	0·007	0·015	0·023	3·537	4·253	5·687
Log–linear ($s_0 = 0{\cdot}001$ m)	0·001	0·0012	0·0014	8·911	9·269	9·632

grid is sufficiently accurate (see currents in Table V, computed in a water depth $h = 100$ m with $\kappa = 14{\cdot}0$).

Similar conclusions with regards to the accuracy of the kappa grid were found when the eddy viscosity was computed using equation (33), in which the viscosity is determined from the current and water depth. Again with this formulation of eddy viscosity an accurate solution could be obtained with five modes in the vertical, which was in good agreement with solutions computed using a logarithmic or log–linear transformed grid (see Table V).

It is apparent from Table V that at a height of 1 m above the sea bed there are significant differences, of order 22 cm s^{-1}, in the D_2-harmonic (40 cm s^{-1} compared with 62 cm s^{-1}) computed from the eddy viscosity related to u^2 rather than hu. Differences of this order are also evident at a height of 5 m above the sea bed. It is also clear from Table V that there are some significant differences in the D_6-component of the current, which is approximately twice as large when the eddy viscosity is related to u^2 rather than hu. However, in a water depth of 100 m, currents computed with the various viscosity options do not exhibit such large differences, e.g. values of 64 compared with 58 cm s^{-1} at 1 m above the bed (see Table V), with smaller differences higher in the water column. Values of the higher harmonic D_6 at 1 m above the bed are again twice as large for the u^2-formulation of viscosity compared with the hu-formulation.

The close agreement of the currents computed with the modal, transformed grid and kappa methods confirms that the differences in current computed using the u^2- and hu-formulations of viscosity are due to physically realistic effects. It is also evident from a comparison of Tables IV and V that in deep water, $h = 100$ m, currents computed with viscosity profile B using a time-independent or time-dependent formulation of viscosity show little difference in magnitude, except in the near-bed region $z = 1$ m where some slight differences are evident, i.e. 60 cm s^{-1} for μ constant, 65 cm s^{-1} for $\mu \propto u^2$ and 58 cm s^{-1} for $\mu \propto hu$. However, in shallow water, $h = 10$ m, at $z = 1$ m significant differences are evident, i.e. 15 cm s^{-1} for μ constant, 39 cm s^{-1} for $\mu \propto u^2$ and 63 cm s^{-1} for $\mu \propto hu$. The large difference in current computed with the hu- and u^2-formulations in a water depth of 10 m suggests that current measurements in such water depths should be able to distinguish between these formulations of eddy viscosity. Also, since the D_6-harmonic is only produced with a time-varying eddy viscosity, some measurements of its value in the near-bed region would be very valuable.

In these calculations, rotational effects were ignored. However, calculations including the influence of rotation showed similar rates of convergence for the modal, logarithmic or log–linear transformed grid and kappa methods.

4. WIND WAVE INDUCED CURRENTS

It is evident from the previous section that the solution of the hydrodynamic equations for tidal flow at a point can be accurately reproduced using either a modal representation or a grid box

through the vertical. In the case of tidal flow the boundary layer thickness can exceed (for $h=10$ m) or be a significant fraction of (for $h=100$ m) the water column. In a wind wave problem, however, the boundary layer thickness is only of order 0·1–0·2 m and consequently is only a small, highly sheared fraction of the water column (see Figure 6). The frequencies of wind waves are significantly higher (typically between 6 and 12 s) than those of tidal waves.

In shallow regions (water depth of order less than 30 m), wind waves have a significant influence upon the bed stress and are particularly important in determining sediment movement. Consequently, in order to be able to accurately predict near-bed currents and stresses in shallow water, the numerical method should be accurate for both wind wave and tidal flows. In this section the accuracy of the numerical methods applied previously for tidal problems are examined for wind wave solutions in which the bottom boundary layer is only a small fraction of the water column.

Wind wave of 8 s period, water depth $h=1$ m. Initially we consider a very shallow region, $h=1$ m. Eddy viscosity profile B is used in these calculations, with $\mu_0=0{\cdot}0001\ \mathrm{m^2\,s^{-1}}$ and $\mu_1=0{\cdot}0050\ \mathrm{m^2\,s^{-1}}$ (a typical value of eddy viscosity[23] for wind waves in shallow water).

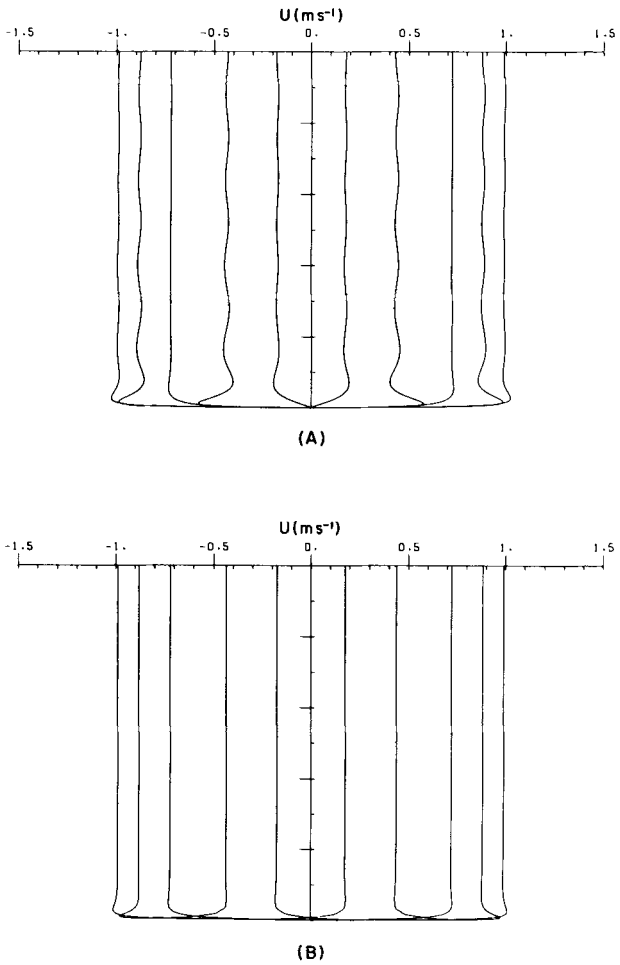

Figure 6. Current profiles at 0·8 s intervals over a wave period ($T=8$ s), computed (A) using 10 modes and (B) using 30 modes

Motion was started from rest by a suddenly applied unit forcing $F_x = 1{\cdot}0$, $G_y = 0{\cdot}0$ in the x-direction of period 8 s^{-1}. A time step of 0·05 s was used in the calculation, giving 160 time steps per wave period. The solution was integrated forward in time for approximately 40 wave periods, by which time the influence of the initial condition of zero motion had been removed and the solution was periodic. The reason for a long integration period can be readily appreciated using equation (32) and appropriate values from Table II, giving $T_D = 271$ s, which for an 8 s^{-1} period wave corresponds to 34 wave periods. The amplitude and phase of the various harmonics were then obtained by harmonic analysis of the current velocities at each time step over a full wave period.

In an initial series of calculations a log–linear transformation was applied in the vertical, with $s_0 = 0{\cdot}001$ m and $s_* = 0{\cdot}5$ m, and a range of grid boxes, N, in the vertical. In a second series of calculations a logarithmic transformation was applied in the vertical, with $s_0 = 0{\cdot}00001$ m. Also, a similar set of calculations were performed using a range of modes. The computed amplitude and phase of the fundamental harmonic at various heights z above the sea bed are given in Table VII.

Table VII. Amplitude h_0 (cm s^{-1}) and phase g_0 (deg) of near-bed wave induced currents computed with a time-independent viscosity in a water depth $h = 1$ m

Height (m)	Number of grid boxes, N							
	10		20		40		60	
	h_0	g_0	h_0	g_0	h_0	g_0	h_0	g_0
Log–linear grid ($s_0 = 0{\cdot}001$ m, $s_* = 0{\cdot}5$ m)								
0·001	5·5	107	3·7	155	2·2	195	1·6	205
0·0025	14·3	239	14·7	239	14·7	239	14·9	239
0·005	32·2	241	32·2	242	32·2	242	32·2	242
0·01	53·0	245	53·3	246	53·8	246	54·1	246
0·1	103·3	265	103·5	265	103·7	266	103·7	266
Logarithmic grid ($s_0 = 0{\cdot}00001$ m)								
0·001	10·9	239	11·4	240	11·5	240	11·6	240
0·0025	23·4	241	24·7	241	24·8	241	24·9	241
0·005	39·8	243	40·0	244	40·5	244	40·6	244
0·01	56·5	246	59·0	247	59·8	247	60·0	247
0·1	101·7	265	103·3	265	103·6	266	103·7	266

Height (m)	Number of modes, M							
	5		10		15		30	
	h_0	g_0	h_0	g_0	h_0	g_0	h_0	g_0
Functional model								
0·001	9·3	258	10·7	249	11·1	245	11·6	241
0·0025	20·2	258	23·2	249	24·1	245	24·9	241
0·005	33·7	258	38·6	249	39·8	246	40·7	243
0·01	51·7	258	58·5	250	59·8	248	59·9	247
0·1	105·6	264	103·1	266	103·3	266	103·3	266

It is evident from this table that the near-bed currents computed with $s_0 = 0{\cdot}001$ m are significantly lower than those determined using the logarithmic transform or the functional model. In the case of $s_0 = 0{\cdot}001$ m the first grid box at which the current is non-zero is only 0·001 m above the sea bed. With such a coarse near-bed grid the high-shear bed layer cannot be resolved and this significantly reduces the currents within the bottom 1 cm of the water column.

Decreasing s_0 to 0·00001 m and using a logarithmic transform in the vertical gives enhanced bed resolution in the model (when $N = 20$ there are 10 grid boxes in the bottom 0·001 m layer). Computed currents based upon the logarithmic transform and the modal method are in excellent agreement, with the order of 10–15 modes being able to resolve the near-bed region.

This calculation clearly shows that for wind wave problems where the bottom boundary layer is particularly thin, of order 10 cm, it is essential to use a small value of s_0 with a transformation that gives maximum resolution in the near-bed layer (i.e. a logarithmic transform). If s_0 is not sufficiently fine then the computed current is incorrect. In the case of the modal model there is no parameter s_0 whose value must be chosen in a subjective manner, and to this extent it has some advantage over the grid box method.

Wind wave of 8 s period, water depth $h = 10$ m. In a second series of calculations the water depth was increased to 10 m and the eddy viscosity μ_1 to 0·1 $m^2 s^{-1}$ to represent a turbulence intensity higher up in the water column, which might occur if wind wave and tidal current were present in combination.

With this water depth it was necessary to integrate for the order of 90000 time steps (over 560 wave periods, i.e. over 1 h) before a periodic solution could be obtained.

As was shown in Section 3, the reason for this can be clearly understood from equation (32), which, using parameters given in Table II, gives T_D of order 0·42 h. For a tidal flow problem where the flow period is of order 12 h the time required for the transients to decay is therefore a fraction of a tidal period. However, for wind wave problems where the wave period is of order 8 s many hundreds of wave periods are required to remove the initial transients.

It is evident from Table VIII that the shear in the near-bed layer (the water column in the bottom 0·01 m) is higher in this calculation than in the previous one. This is because the layer thickness h_1 is a fixed fraction of the water column, and consequently when the water depth increases, the low-viscosity near-bed layer increases in thickness. This is certainly a deficiency of the present model in that physically the thickness of this near-bed layer would probably be independent of water depth. Although the viscosity profile used in this calculation may be physically unrealistic, it does demonstrate that an accurate solution can be obtained with the modal approach, although the number of modes required is larger than in the previous example (see Table VIII).

Comparing the modal solutions in Tables VII and VIII, it is evident that the current 0·01 m above the bed can be accurately computed in a water depth of 1 m by using 15 modes in the vertical, whereas in a water depth of 10 m the modal solution converges more slowly, with 30 modes required to give a solution comparable to that obtained with the logarithmic transform at a height of 0·01 m.

It is also clear from Table VIII that an accurate solution can be obtained using a log–linear transform provided that s_0 is sufficiently fine (i.e. $s_0 = 0{\cdot}0001$ m).

Wind wave of 8 s period, water depth $h = 10$ m, time-dependent viscosity. As with the tidal problem, it is probably more physically realistic to assume that the eddy viscosity will evolve over the wave period, using equation (33) or (34) to relate the viscosity to the flow field.

Table VIII. Amplitude h_0 (cm s^{-1}) and phase g_0 (deg) of near-bed wave induced ($T=8$ s^{-1}) currents computed with a time-independent viscosity in a water depth $h=10$ m

Height (m)	Number of grid boxes, N							
	10		20		40		60	
	h_0	g_0	h_0	g_0	h_0	g_0	h_0	g_0
Logarithmic grid ($s_0=0{\cdot}00001$ m)								
0·01	56·9	249	60·5	250	61·5	250	61·7	250
0·025	81·8	254	84·5	254	84·8	254	84·8	254
0·05	95·7	258	99·1	259	98·9	259	99·0	259
0·10	105·6	262	108·2	263	107·8	263	107·9	263
1·00	107·7	269	107·7	269	107·6	269	107·6	269
Log–linear grid ($s_0=0{\cdot}0001$ m, $s_*=5{\cdot}0$ m)								
0·01	57·4	249	60·2	250	61·1	250	61·1	250
0·025	79·5	253	83·1	254	84·3	254	84·6	254
0·05	98·7	258	97·8	258	98·8	258	99·0	259
0·10	104·4	262	107·2	263	107·9	263	107·8	263
1·00	107·9	269	107·6	269	107·6	269	106·7	269

Height (m)	Number of modes, M							
	5		10		15		30	
	h_0	g_0	h_0	g_0	h_0	g_0	h_0	g_0
Eigenfunction model								
0·01	39·1	267	49·9	262	54·7	256	58·5	250
0·025	56·6	267	71·4	262	77·4	258	80·2	254
0·05	70·4	267	87·1	263	92·3	259	93·0	259
0·10	83·7	267	99·4	264	101·7	262	100·8	264
1·00	104·2	268	99·0	269	100·1	268	99·9	269

In a final series of calculations the current amplitude and phase were computed in a water depth of 10 m using eddy viscosity profile B and the same form and time variation of viscosity used for the tidal flow problem. Solutions were computed using 30 modes in the vertical, and 60 grid boxes based on both logarithmic and log–linear transforms with various values of s_0 and s_* (Table IX).

It is evident from Table IX that the currents computed using a finite difference grid are essentially independent of the transformation used, provided s_0 is sufficiently small. The currents computed using the modal representation through the vertical, although of the order of 5 cm s^{-1} smaller in the upper part of the bottom boundary layer, are in general in good agreement, particularly in the high-shear bottom layer, with those computed using a grid representation in the vertical.

The good agreement between the modal representation and that using a transformed grid is particularly encouraging, since in this case the bottom boundary layer has a thickness of only 0·1 m, i.e. only occupies 1% of the water column. In such cases a logarithmic transform in which maximum resolution is concentrated within this bottom boundary layer would be optimal, since

Table IX. Amplitude h_0 (cm s^{-1}) and phase g_0 (deg) of near-bed wave induced currents computed with a time-dependent viscosity using viscosity profile **B** in a water depth $h = 10$ m

Height (m)	$\mu \propto u^2$								$\mu \propto hu$							
					Log–linear								Log–linear			
	Modes 30		Logarithmic $s_0 = 0{\cdot}00001$ m		$s_0 = 0{\cdot}0001$ m $s_* = 5{\cdot}0$ m		$s_0 = 0{\cdot}00001$ m $s_* = 2{\cdot}5$ m		Modes 30		Logarithmic $s_0 = 0{\cdot}00001$ m		$s_0 = 0{\cdot}0001$ m $s_* = 5{\cdot}0$ m		$s_0 = 0{\cdot}00001$ m $s_* = 2{\cdot}5$ m	
	h_0	g_0	h_0	g_0	h_0	g_0	h_0	g_0	h_0	g_0	h_0	g_0	h_0	g_0	h_0	g_0
D_2																
0·01	69·2	237	70·7	237	70·4	237	70·8	237	89·1	249	93·6	248	93·1	248	93·6	248
0·025	87·4	246	90·2	245	90·3	245	90·4	245	103·1	259	108·7	259	108·7	259	108·7	259
0·05	95·6	254	100·9	252	101·1	252	101·1	252	102·6	268	111·0	266	111·1	266	111·1	266
0·10	101·3	260	107·6	259	107·7	259	107·6	259	101·1	269	108·9	269	109·0	269	108·9	269
1·00	99·9	269	107·6	269	107·7	269	107·7	269	100·0	269	107·6	269	107·7	269	107·7	269
D_6																
0·01	10·0	244	10·7	240	10·8	241	10·8	242	4·1	271	4·9	272	5·0	271	4·9	272
0·025	7·4	266	8·2	264	8·3	265	8·2	266	1·6	317	2·0	335	2·0	334	2·0	336
0·05	4·5	309	5·4	291	5·4	292	5·4	293	1·5	52	1·0	43	1·0	43	1·0	43
0·10	2·1	338	2·9	330	3·0	331	3·0	331	0·3	196	0·3	101	0·0	0·0	0·0	0·0
1·00	0·0	211	0·0	173	0·0	0·0	0·0	0·0	0·0	58	0·0	179	0·0	0·0	0·0	0·0

above this layer (see Figure 6) there is no shear in the water column and minimum resolution is required. It is evident from Figure 6, profiles A and B, that the wave induced currents computed with 10 modes ($M=10$, profile A) exhibit physically unrealistic ripples above the bottom boundary layer. However, when the number of modes is increased to 30, these ripples disappear (see Figure 6, profile B) and the high-shear bottom boundary layer is reproduced. The fact that the modal model can reproduce this high-shear bottom boundary with the order of 30 modes, coupled with the computational economy of the method and the insight associated with it, is particularly valuable.

Again, as with the tidal problem, it is evident that close to the bed (i.e. 0·025 m above it) there are some differences in current magnitude (i.e. 85 cm s^{-1} for μ constant, 90 cm s^{-1} for $\mu \propto u^2$ and 108 cm s^{-1} for $\mu \propto hu$) depending upon the eddy viscosity formulation. Also of particular interest is the second harmonic (D_6), which is absent in the time-invariant viscous flow problem but is significantly larger when $\mu \propto u^2$ than when $\mu \propto hu$ (see Table IX).

It appears unlikely that open sea measurements will be able to measure with accuracy currents only 2·5 cm above the sea bed. Also, in many cases, ripples on the sea bed would be comparable in magnitude. However, laser Doppler current meters in laboratory flumes should be able to make such near-bed measurements, which hopefully would distinguish these various formulations of viscosity.

5. CONCLUDING REMARKS

In this paper a point model through the vertical has been used to assess the accuracy and computational efficiency of using a finite difference grid or a modal representation through the vertical in determining the profile of tidal or wind wave induced currents.

A no-slip condition was applied at the sea bed, and with a physically realistic profile of eddy viscosity a resulting high-shear bottom boundary layer occurred. In order to accurately resolve this high-shear layer, a logarithmic or log–linear transformation was used in the vertical before applying a uniform finite difference grid on the transformed co-ordinate. An alternative to transforming in the vertical was the application of an irregular finite difference grid with grid spacing graded to retain second-order accuracy (a kappa grid). By varying the rate of change of the grid spacing, a very fine grid in the near-bed region was obtained.

In an alternative approach a modal method was used in the vertical. These modes were computed in terms of an expansion of 60 B-splines based upon a knot distribution with high resolution in the bottom boundary layer. By this means a set of modes were computed which could accurately resolve the high-shear near-bed layer.

Calculations showed that in the case of tidal currents, where the high-shear bottom boundary layer extended through the water column or was a significant fraction of it, an accurate solution could be obtained using five to 10 modes. Finite difference solutions of comparable accuracy required the order of 20 grid boxes on a log–linear transformed co-ordinate. An accurate solution could also be obtained using an irregularly spaced grid in the vertical (the kappa method). However, a high value of kappa ($\kappa > 10$) with a significantly larger number (order 60) of grid boxes than that used with the log–linear transformation was required.

In the case of a wind wave problem, the high-shear layer is confined to the near-bed region, and in a water depth of order 10 m occupies only 1% of the water column. A uniform finite difference grid on a logarithmic transformed co-ordinate appeared optimal in this case since it gives maximum resolution in the high-shear bottom boundary layer.

The modal method also gave a solution of acceptable accuracy in this problem provided the number of modes was of order 30—a significantly larger number than the five modes required for

tidal flow in this water depth. It is evident from these calculations that the critical parameter controlling the number of modes required in the solution is the ratio of shear boundary layer thickness to water depth. When this ratio is small (of order 1%) it appears that the order of 30 modes or more is required, whereas when the boundary layer thickness is comparable to the water depth an accurate solution can be obtained with five modes. Certainly when the ratio is small, the finite difference method with a logarithmic transformed co-ordinate is optimal in the sense that a smaller number N of grid boxes than modes M are required in the vertical. Although more modes are required than grid boxes in this case, the computational efficiency of the modes[16] coupled with the ability to produce highly vectorizable algorithms based upon them[17] makes their application particularly attractive on vector-processing computers. Also, for problems involving wave–current interaction, both wave and current boundary layers will co-exist and the logarithmic transform will no longer be optimal.

The principal difficulty with the modal method is that although the magnitude of eddy viscosity can vary with horizontal position and time, the profile of viscosity has to remain constant unless the modes are to be recomputed during the course of the calculation, with the associated high computational cost. However, three-dimensional simulations of tidal flow on the European Continental Shelf using a no-slip bottom boundary condition and a modal method in the vertical suggest that, provided a physically realistic profile of viscosity is used, the computed current profiles are in good agreement with observations. Further calculations and comparisons using this three-dimensional model are presently in progress and will be reported in due course.

The calculations presented in this paper show clearly that the computed tidal current profiles determined using a constant eddy viscosity in the vertical are significantly different in shallow water than those computed using a near-bed reduction in eddy viscosity. Also, significant differences (particularly in shallow water) are found between current profiles computed with time-varying and time-independent viscosity.

The fact that the currents computed with the modal, transformed grid and kappa methods are in close agreement confirms that the differences in current computed using the u^2- and hu-formulations of viscosity are due to physically realistic effects. The large differences in current found with these two different formulations in a water depth of 10 m suggest that current measurements in such water depths could distinguish between these viscosity formulations. Also, the fact that the third harmonic (D_6) is only produced with a time-varying viscosity indicates that measurements of its value in the near-bed region would also yield significant insight into the viscosity formulation. By this means, appropriate formulations of eddy viscosity could be verified by a combination of models and measurements.

ACKNOWLEDGEMENTS

The author is indebted to Mr. R. A. Smith for preparing the diagrams used in the paper. The care taken by Mrs. J. Hardcastle in typing the text is appreciated.

REFERENCES

1. A. Owen, 'A three-dimensional model of the Bristol Channel', *J. Phys. Oceanogr.*, **10**, 1290–1302 (1980).
2. M. Spaulding, T. Isaji, D. Mendelsohn and A. C. Turner, 'Numerical simulation of wind-driven flow through the Bering Strait', *J. Phys. Oceanogr.*, **17**, 1799–1816 (1987).
3. A. M. Davies, 'A three-dimensional model of the Northwest European Continental Shelf, with application to the M_4 tide', *J. Phys. Oceanogr.*, **16**, 797–813 (1986).
4. A. M. Davies and G. K. Furnes, 'Observed and computed M_2 tidal currents in the North Sea', *J. Phys. Oceanogr.*, **10**, 237–257 (1980).

5. A. M. Davies, 'Spectral models in continental shelf sea oceanography', in N. S. Heaps (ed.), *Three-Dimensional Coastal Ocean Models*, AGU, Washington, D.C., 1987, pp. 71–106.
6. R. B. Gordon and M. L. Spaulding, 'Numerical simulations of the tidal- and wind-driven circulation in Narragansett Bay', *Estuarine, Coastal and Shelf Sci.*, **24,** 611–636 (1987).
7. M. L. Spaulding and T. Isaji, 'Three dimensional continental shelf hydrodynamic model including wave current interaction', in J. C. J. Nihoul and B. M. Jamart (eds), *Three-Dimensional Models of Marine and Estuarine Dynamics*, Elsevier, Amsterdam, 1987, pp. 405–426.
8. B. M. Jamart and J. Ozer, 'Comparison of 2-D and 3-D models of the steady wind-driven circulation in shallow water', *Coastal Eng.*, **11,** 393–414 (1987).
9. A. M. Davies, 'On formulating two-dimensional vertically integrated hydrodynamic numerical models with an enhanced representation of bed stress', *J. Geophys. Res.*, **93,** 1241–1263 (1988).
10. G. K. Furnes and M. Mork, 'Formulation of a continuously stratified sea model with three-dimensional representation of the upper layer', *Coastal Eng.*, **11,** 415–445 (1987).
11. J. Noye, 'Finite difference techniques for partial differential equations', in B. Noye (ed.), *Computational Techniques for Differential Equations*, North-Holland, Amsterdam, 1984, pp. 95–354.
12. J. Noye and M. Stevens, 'A three-dimensional model of tidal propagation using transformations and variable grids', in N. S. Heaps (ed.), *Three-Dimensional Coastal Ocean Models*, AGU, Washington, D.C., 1987, pp. 41–70.
13. A. M. Davies, 'Application of the Dufort–Frankel and Saul'ev methods with timesplitting to the formulation of a three dimensional hydrodynamic sea model', *Int. j. numer. methods fluids*, **5,** 405–425 (1985).
14. F. G. Schuman, 'Numerical methods in weather prediction: II—Smoothing and filtering', *Mon. Weather Rev.*, **85,** 357–361 (1957).
15. A. M. Davies, 'Formulation of a linear three-dimensional hydrodynamic sea model using a Galerkin–eigenfunction method', *Int. j. numer. methods fluids*, **3,** 33–60 (1983).
16. A. M. Davies and C. V. Stephens, 'Comparison of the finite difference and Galerkin methods as applied to the solution of the hydrodynamic equations', *Appl. Math. Modelling*, **7,** 226–240 (1983).
17. A. M. Davies and R. Proctor, 'Developing and optimizing a 3D-spectral/finite difference hydrodynamic model for the CRAY X-MP', *Comput. Fluids*, in the press.
18. A. M. Davies, 'A three-dimensional modal model of wind induced flow in a sea region', *Prog. Oceanogr.*, **15,** 71–128 (1985).
19. K. F. Bowden, L. A. Fairbairn and P. Hughes, 'The distribution of shearing stresses in a tidal current', *Geophys. J. R. Astron. Soc.*, **2,** 288–305 (1959).
20. K. W. Bowden and S. R. Ferguson, 'Variations with height of the turbulence in a tidally induced bottom boundary layer', in J. C. J. Nihoul (ed.), *Marine Turbulence, Proc. 11th Liege Colloq. on Ocean Hydrodynamics, Elsevier Oceanography Ser. Vol. 28*, Elsevier, Amsterdam, 1980, pp. 259–286.
21. A. M. Davies and J. E. Jones, 'On the numerical solution of the turbulence energy equations for wave and tidal flows', *Int. j. numer. methods fluids*, **12,** 17–41 (1991).
22. R. W. Lardner and H. M. Cekirge, 'A new algorithm for three-dimensional tidal and storm surge computations', *Appl. Math. Modelling*, **12,** 471–481 (1988).
23. A. M. Davies and J. E. Jones, 'Modelling turbulence in shallow sea regions, in J. C. J. Nihoul and B. M. Jamart (eds), *Small-Scale Turbulence and Mixing in the Ocean, Proc. 19th Liege Colloq. on Ocean Hydrodynamics*, Elsevier, Amsterdam, 1987, pp. 63–76.